

STRUCTURAL AND DIELECTRIC STUDIES OF $Zn_{0.5}Mg_{0.5}Pr_xFe_{2-x}O_4$ FERRITES**S. Singh^{1*} and S. Ram²**^{1,2}Material Science Laboratory, Department of Physics, J. N. V. University Jodhpur*Corresponding author: ¹shailndrasingh89@gmail.com**ABSTRACT**

The Zn-Mg spinel ferrite doped with Praseodymium samples at nanoscale of general formula $Zn_{0.5}Mg_{0.5}Pr_xFe_{2-x}O_4$ ($x=0.02, 0.06, 0.10$) have been prepared by standard solid state reaction technique using high purity oxides. X-ray diffraction analysis shows the formation of a Zn-Mg ferrite cubic phase at room temperature with space group $Fd3m$. Lattice constant is increased with Pr^{+3} substitution increases. FTIR spectra show two significant absorption bands first at $\sim 565\text{ cm}^{-1}$ and second at 434 cm^{-1} to 451.3 cm^{-1} which were respectively attributed to tetrahedral (A) and octahedral (B) sites of the spinel. SEM and EDS results show that the particles are homogeneous with spherical manner without any impurity pickup. The dielectric measurements were carried out at room temperature as a function of frequency. The experimental results show that dielectric constant and dielectric loss decrease as frequency increases.

Keywords: XRD, FTIR, Tetrahedral and Octahedral**Introduction**

Spinel ferrites with the general formula MFe_2O_4 shows interesting structural, magnetic and electrical properties that vary with the nature of ions and the site distribution among tetrahedral and octahedral sites. Their characteristics widely vary with the method and the conditions of preparation [1]. Diverse practical applications of spinel ferrites have attracted the attention of researchers for decades. The properties of the ferrites in the nano-regime differ much from the bulk. The study of spinel ferrites in the nano-regime is significant because of their interesting magnetic and electrical properties [2]. Ferrites substituted with different cations prepared by various techniques exhibit interesting applications and involve exciting physics in them. There are several methods for synthesizing nano-sized spinel ferrites, such as co-precipitation, sol-gel, micro-emulsion, hydrothermal and the solid state reaction method [3, 4]. Due to the good stoichiometric control and production of ultrafine particles in the nano-range, the solid state reaction technique is an attractive preparation method [5].

The crystalline structure of the spinel ferrites has two sites, the tetragonal A-sites and octahedral B-sites. The zinc ferrite, $ZnFe_2O_4$, has the normal spinel structure, in which the Zn^{+2} ions occupy the tetrahedral sites where the octahedral B-sites are occupied by the Fe^{+3} ions. Magnesium ferrite, $MgFe_2O_4$ is

predominantly an inverse spinel and the degree of inversion depends upon heat treatment [6].

Substitution of rare-earth ions into the spinel structure results in structural distortion and induces strains that significantly modify electrical and magnetic properties [7-9]. Many researchers have investigated the physical and structural properties of such ferrites because substitution of a small proportion of rare-earth elements with large ionic radii in ferrites will drastically modify its properties. But seldom have studies been reported in Pr^{+3} ions substituted nano-sized zinc-magnesium ferrite [10].

Our investigation on the structural, morphological and electrical properties of Pr^{+3} ions replacing Fe^{+3} ions in nano-sized zinc-magnesium ferrite was able to throw light on the doping concentration limit to obtain single-phase ferrite. Synthesis of nano-sized ferrites was performed using a high temperature solid state reaction technique. X-ray diffraction (XRD), Fourier transform infrared (FTIR) and were performed for studying the structural characteristics. Scanning electron microscope (SEM) measurements were taken for surface morphology, Energy Dispersive X-Ray Analysis (EDX), were used to elemental analysis. LCR meter were used to dielectric analysis. XRD analysis reveals a limit for Pr^{+3} concentrations to obtain pristine $Zn_{0.5}Mg_{0.5}Fe_{2-x}Pr_xO_4$ without any extra phase. The FTIR spectrum shows the substitution of Fe^{+3} ions on octahedral B-sites by Pr^{+3} ions. The dielectric

results reveal that dielectric constant and dielectric loss decrease as frequency increases.

Experimental

The Zn-Mg spinel ferrite of general formula $Zn_{0.5}Mg_{0.5}Pr_xFe_{2-x}O_4$ (where $x = 0.02, 0.06, 0.10$) was synthesized by the method of high temperature solid state reaction technique under controlled condition of time and temperature. Stoichiometric amount of ZnO, MgO, Fe_2O_3 and Pr_2O_3 powder were mixed thoroughly in liquid medium and calcined at $600^\circ C$ for 8 hours in a silica crucible. The process of grinding and calcinations was repeated for a number of times until a fine homogeneous sample of the material was obtained. Finally, the sintering of the pellets and powder was done at high temperature i.e. $1180^\circ C$ [11].

X-ray diffraction data at room temperature were collected at $2^\circ/\text{min}$ scanning rate from 10° to 80° range of 2θ on PANalytical X'pert Pro MPD diffractometer of Cu- $K\alpha$ radiation. The lattice constant and d-spacing were calculated. Fourier transforms infrared spectroscopy (FTIR) was used to analyze the intrinsic vibrational frequency of the tetrahedral and

octahedral sites of the spinel structure in the range of 400 to 4000 cm^{-1} with FTIR interferometer IR prestige-2. SEM with EDS was used to assess the surface morphology, grain size and elemental characterization of all synthesized samples using the Nova Nano FE-SEM 450 (FEI). Dielectric studies were carried out by using Hioki 3532-50 LCR Hi-Tester. The dielectric constant and dielectric loss were measured as a function of frequency from 1 kHz to 1 MHz .

Result and Discussion

X-ray diffraction analyses have been performed on the series of $Zn_{0.5}Mg_{0.5}Pr_xFe_{2-x}O_4$ (where $x = 0.02, 0.06, 0.10$) ferrite samples to study their structural phase and the respective XRD patterns are given in Figure 1. The XRD patterns reveal the cubic spinel structure with space group $Fd3m$. The diffraction planes are analyzed with "FullPROOF" software [12]. The planes are indexed as (111), (220), (311), (400), (422), (511) and (440) which are well matched with the earlier reports of pure Zn-Mg ferrite [13]. The broadening and low intensity of diffraction peaks is attributed to presence of ultrafine particles in the samples.

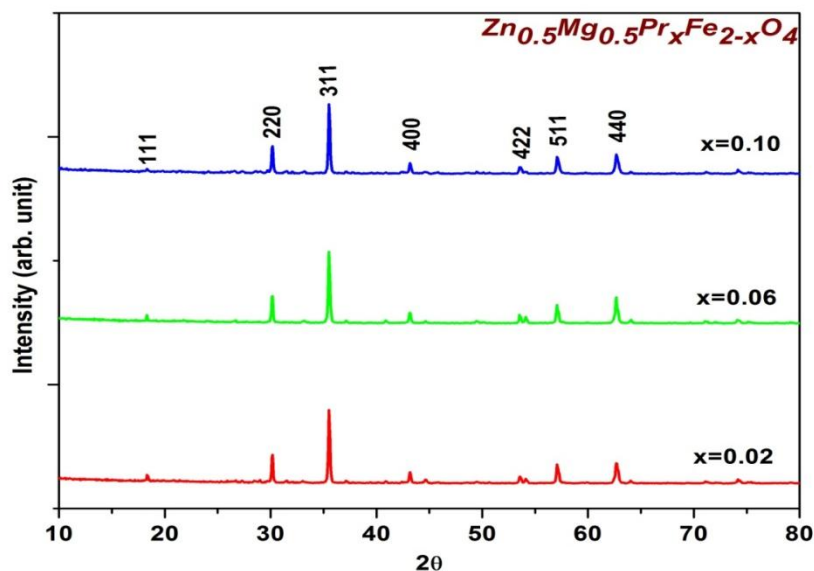


Figure: 1 X-ray powder diffraction pattern of $Zn_{0.5}Mg_{0.5}Pr_xFe_{2-x}O_4$ (where $x=0.02, 0.06, 0.10$)

Figure 2-4 depicts the Rietveld refinement of an X-ray powder diffraction pattern for $Zn_{0.5}Mg_{0.5}Pr_xFe_{2-x}O_4$ (where $x=0.02, 0.06, 0.10$) ferrites at room temperature using the "FullPROOF" software. To simulate the peak profile based on the $Fd3m$ (227) space group, a

pseudo-Voigt function twisted with an axial divergence symmetry function was employed. The produced pattern adequately reproduces all of the observed reflections and yielded a nearly similar reliability factor. Using the Rietveld technique, there is excellent agreement

between the observed and predicted diffraction pattern. Table 1 summarized the lattice constant and other improved characteristics of the produced samples using the solid state reaction method and we observed that the lattice constant is increases with the increasing

of substitution of Pr^{+3} ions see Figure 5. This is may be due to larger ionic radii of Pr^{+3} ($\sim 1.13\text{\AA}$) as compare to ionic radii of Fe^{+3} ($\sim .60\text{\AA}$) [11].

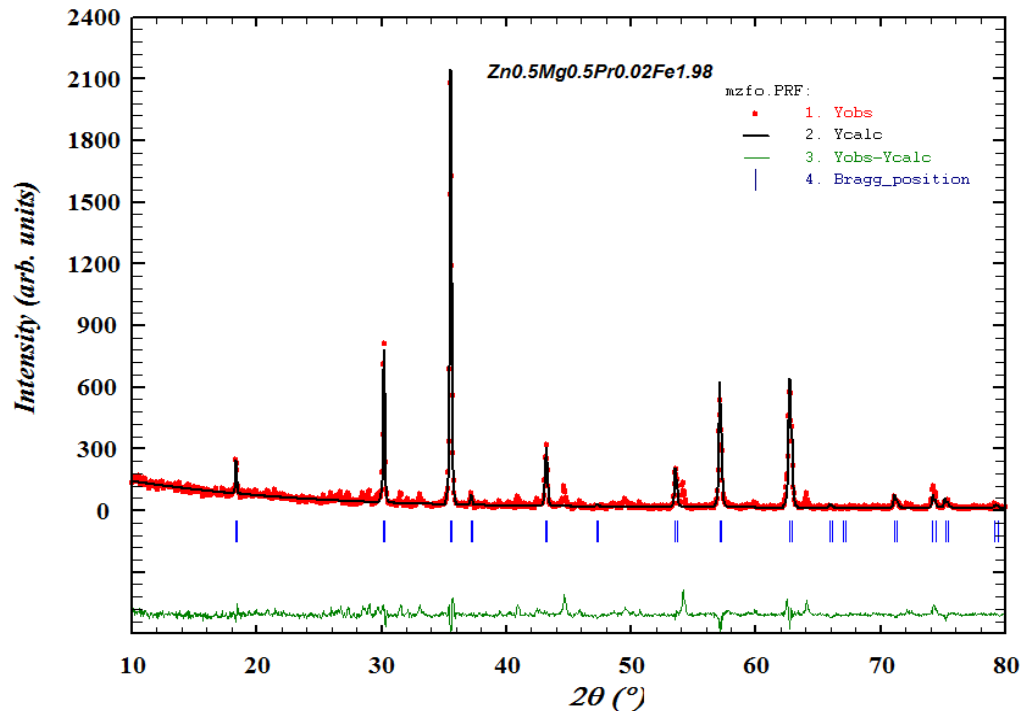


Figure 2: Rietveld refined profile of $\text{Zn}_{0.5}\text{Mg}_{0.5}\text{Pr}_{0.02}\text{Fe}_{1.98}\text{O}_4$

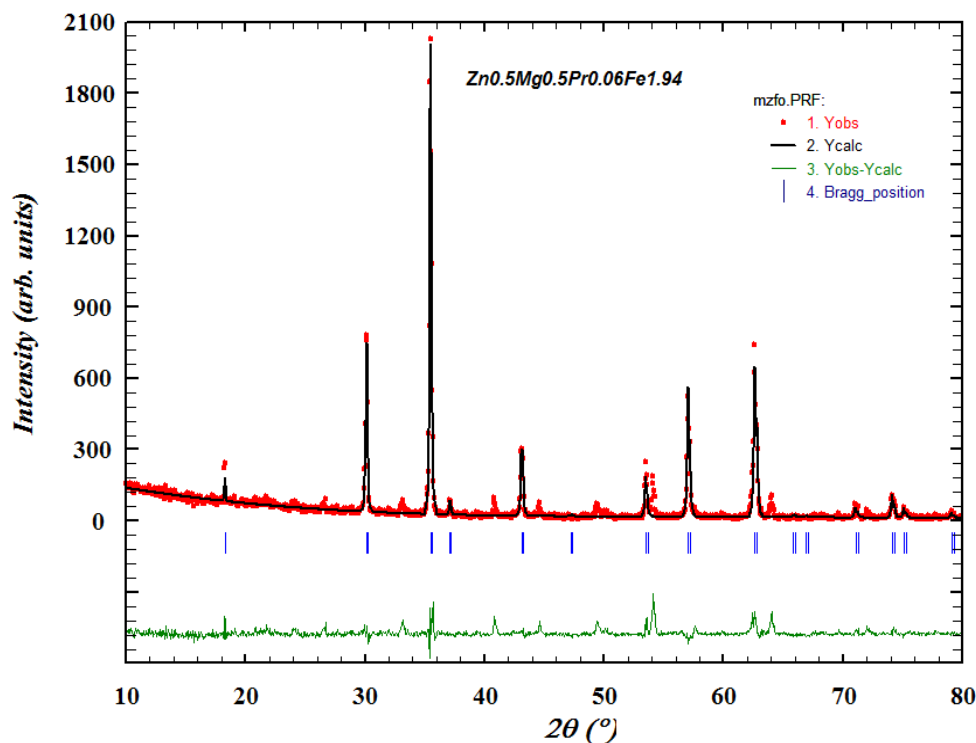


Figure 3: Rietveld refined profile of $\text{Zn}_{0.5}\text{Mg}_{0.5}\text{Pr}_{0.06}\text{Fe}_{1.94}\text{O}_4$

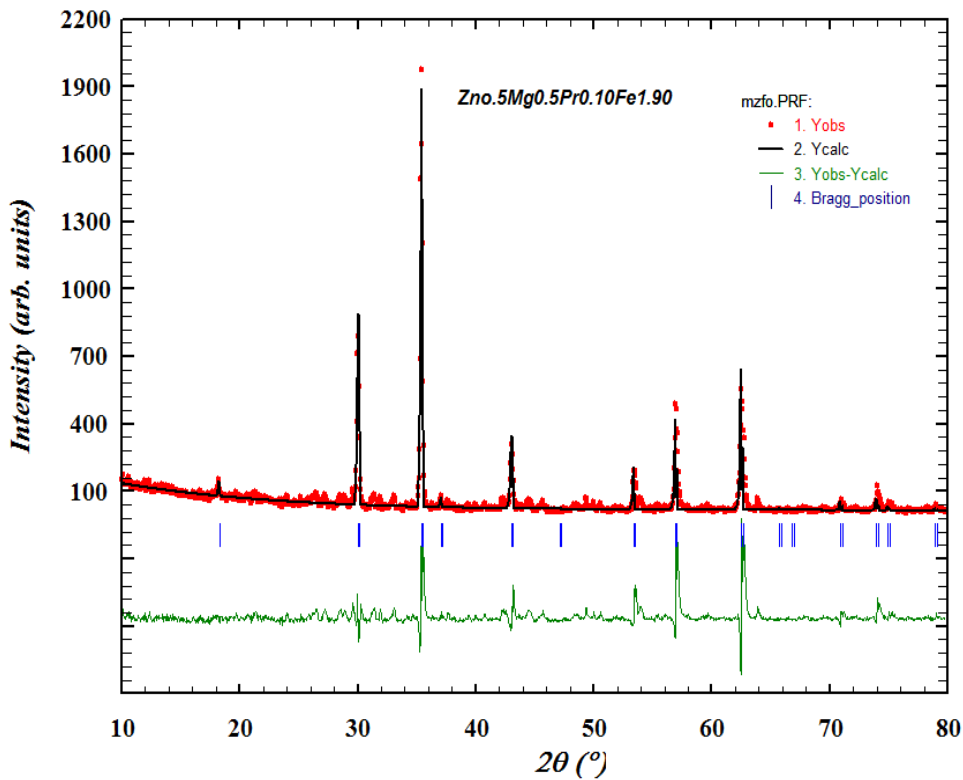


Figure 4: Rietveld refined profile of $Zn_{0.5}Mg_{0.5}Pr_{0.10}Fe_{1.90}O_4$

Table 1: Detailed Rietveld refinement of the room temperature X-ray powder Diffraction patterns of $Zn_{0.5}Mg_{0.5}Pr_xFe_{2-x}O_4$ ($X=0.02, 0.06$ and 0.10) Pr^{+3} -ion concentration on Fe^{+3} -site in ferrit.

Structural parameters	X=0.02	X=0.06	X=0.10
Formula Weight	222.2348	225.6373	229.0398
2θ (degree) range	10-80	10-80	10-80
Step size	0.05	0.05	0.05
Crystal symmetry	Cubic	Cubic	Cubic
Space group	Fd3m	Fd3m	Fd3m
Point group	m-3m	m-3m	m-3m
Lattice parameters a=b=c (Å)	8.3762	8.3825	8.3997
Unit cell volume (Å ³)	587.692	589.023	592.642
U	0.052682	0.022563	0.036072
V	-0.018306	-0.017482	-0.016656
W	0.017745	0.020153	0.003224
Bragg R-factor	8.89	9.51	33.9
Rf-factor	9.92	10.2	28.3
χ^2	3.68	3.94	7.96
GoF	1.9	1.9	2.8

The observed (from the XRD pattern) and estimated (based on the revised cell parameter) inter-planer spacing (d-values) of h k l planes is consistent, as shown in Table 2. According

to the table, there is a considerable rise in the inter-planer spacing value with Pr^{+3} doping ions, which is related to the increase in ionic radii.

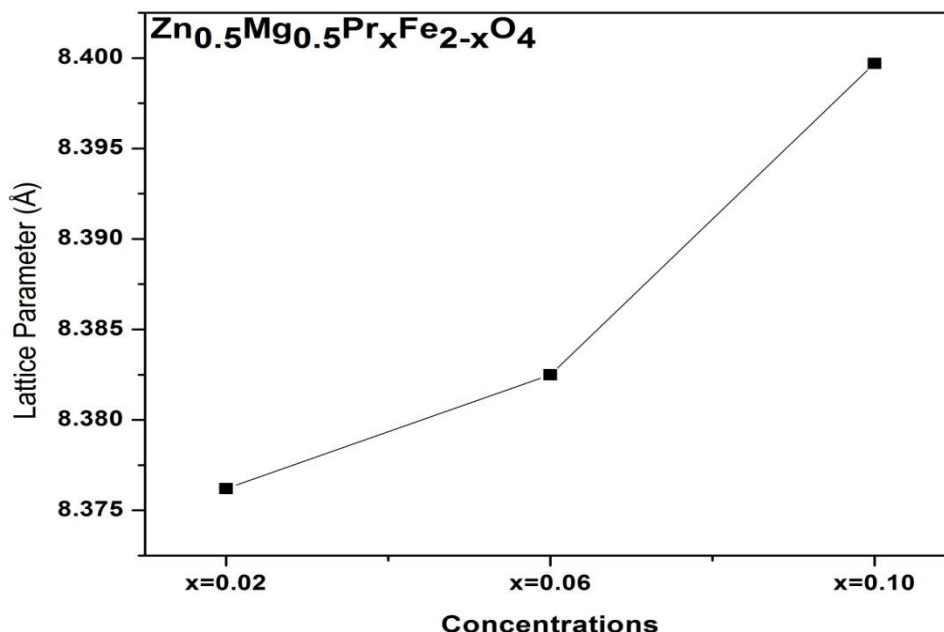


Figure: 5 variations in lattice constant with Pr concentrations.

Table 2: Comparison between some of the observed and calculated d-values (Å) for Zn_{0.5}Mg_{0.5}Pr_xFe_{2-x}O₄ (X= 0.02, 0.06 and 0.10) after Rietveld refinement.

X=0.02		X=0.06		X=0.10		hkl
d _{obs}	d _{cal}	d _{obs}	d _{cal}	d _{obs}	d _{cal}	
4.83588	4.836	4.839545	4.8397	4.84952	4.8496	111
2.96136	2.9614	2.963568	2.9636	2.969635	2.9697	220
2.525432	2.5255	2.527361	2.5274	2.532541	2.5326	311
2.417957	2.418	2.41978	2.4198	2.424695	2.4248	222
2.093978	2.094	2.09555	2.0956	2.099862	2.0999	400
1.921605	1.9216	1.923024	1.9231	1.926987	1.927	331
1.709753	1.7098	1.711026	1.711	1.714529	1.7146	422
1.611963	1.612	1.61318	1.6132	1.616477	1.6165	333
1.611963	1.612	1.61318	1.6132	1.616477	1.6165	511
1.480688	1.4807	1.481792	1.4818	1.484838	1.4848	440
1.4158	1.4158	1.416868	1.4169	1.419777	1.4198	531
1.396	1.396	1.39705	1.3971	1.399917	1.3999	442
1.324369	1.3244	1.325356	1.3254	1.328067	1.3281	620
1.277321	1.2773	1.27828	1.2783	1.280902	1.2809	533
1.262734	1.2627	1.263679	1.2637	1.266268	1.2663	622
1.208966	1.209	1.209873	1.2099	1.212361	1.2124	444

Figure 6 show infrared spectra of Zn_{0.5}Mg_{0.5}Fe_{2-x}Pr_xO₄ (where x =0.02, 0.06, 0.10). There are two significant absorption bands in the ~565cm⁻¹ and 424–451.3 cm⁻¹ range. Waldron reported these two bands for spinel ferrites [14]. The higher band frequency (ν₁) is given to Fe³⁺-O²⁻ stretching vibrations at

the tetrahedral site (A), whereas the lower band frequency (ν₂) is attributed to Fe³⁺-O²⁻ stretching vibrations at the octahedral site (B). Tables 3 show the tetrahedral and octahedral vibrational frequencies (ν₁ and ν₂), as well as the tetrahedral and octahedral force constants (K_t and K_o).

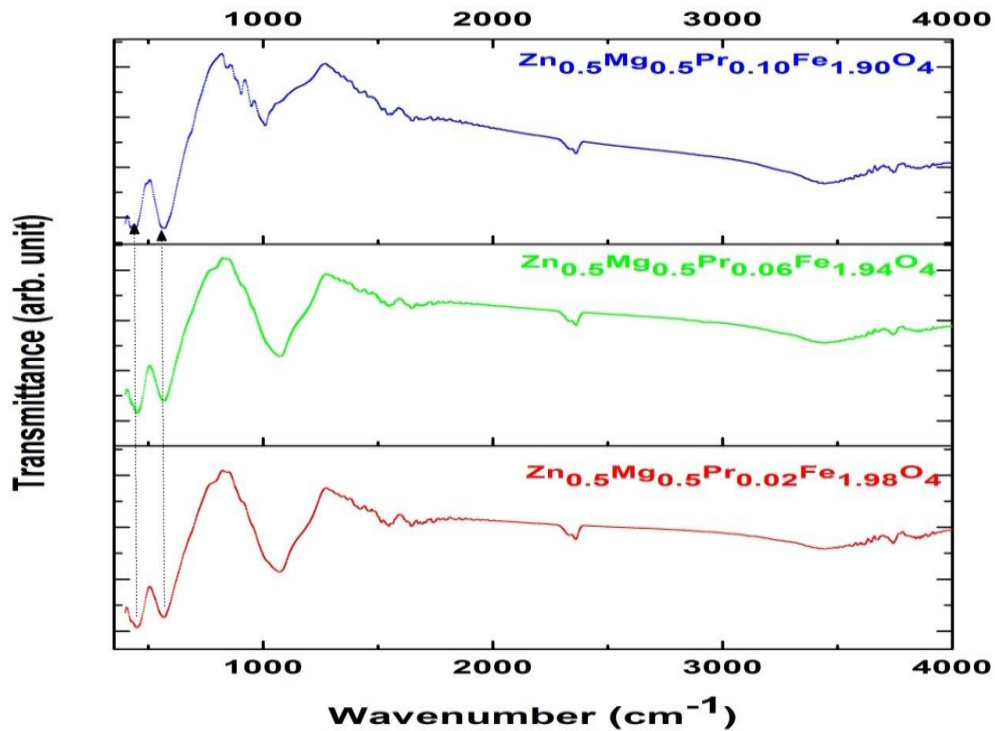


Figure: 6 FT-IR spectra of $Zn_{0.5}Mg_{0.5}Pr_xFe_{2-x}O_4$ (where $x=0.0, 0.02, 0.06, 0.10$)

The formula was used to determine the force constants.

$$K = 4\pi^2 c^2 \nu^2 \mu$$

Where c is the speed of light (2.99×10^{10} cm/s), ν is the vibration frequency of the A-site and B-sites, and μ is the reduced mass of the Fe^{3+} and O^{2-} ions (2.601×10^{-23} g).

Table: 3 IR Band positions ν_1 and ν_2 , force constants K_t and K_o for prepared $Zn_{0.5}Mg_{0.5}Pr_xFe_{2-x}O_4$ (where $x=0.02, 0.06, 0.10$) ferrites.

X	ν_1 (cm ⁻¹)	ν_2 (cm ⁻¹)	$K_t * 10^5$ (dynes/cm)	$K_o * 10^5$ (dynes/cm)
0.02	564.44	450.2	2.9413E-05	1.8712E-05
0.06	564.89	451	2.946E-05	1.8778E-05
0.1	565.55	451.3	2.9529E-05	1.8803E-05

The band frequency ν_2 rises and broadens with Pr^{3+} concentration, however ν_1 does not vary significantly and just a little broadening is seen, which may be due to the substitution of Fe^{3+} ions on octahedral B-sites by Pr^{3+} ions. The bands 3750cm^{-1} and 1550cm^{-1} correspond to stretching and bending vibrations of H–O–H, indicating the existence of free or absorbed water.

Figure 7-9 are a SEM micrograph of $Zn_{0.5}Mg_{0.5}Pr_xFe_{2-x}O_4$ (where $X=0.02, 0.06, 0.10$) at various magnifications. The SEM micrograph surface morphology shows that the grain distribution is not uniform throughout the surface of the ferrite samples. The grain size estimated from the micrograph is $15\mu\text{m}$ to

$20\mu\text{m}$, indicating that optimizing time and temperature during the sintering process enhanced grain packing and distribution throughout the sample (15).

The grain size increases from $15\mu\text{m}$ to $20\mu\text{m}$. This increase in grain size caused by an increase in Pr^{3+} ion concentration may be explained by the difference in ionic radii of Pr^{3+} and Fe^{3+} . Because the size of the Pr^{3+} ion is lower than that of the Fe^{3+} ion, the grain size of Pr^{3+} substituted compounds rises as the concentration of Pr^{3+} ion in the compounds increases. Not only that, but when the concentration of Pr^{3+} ions increases, the grains become more spherical and uniform.

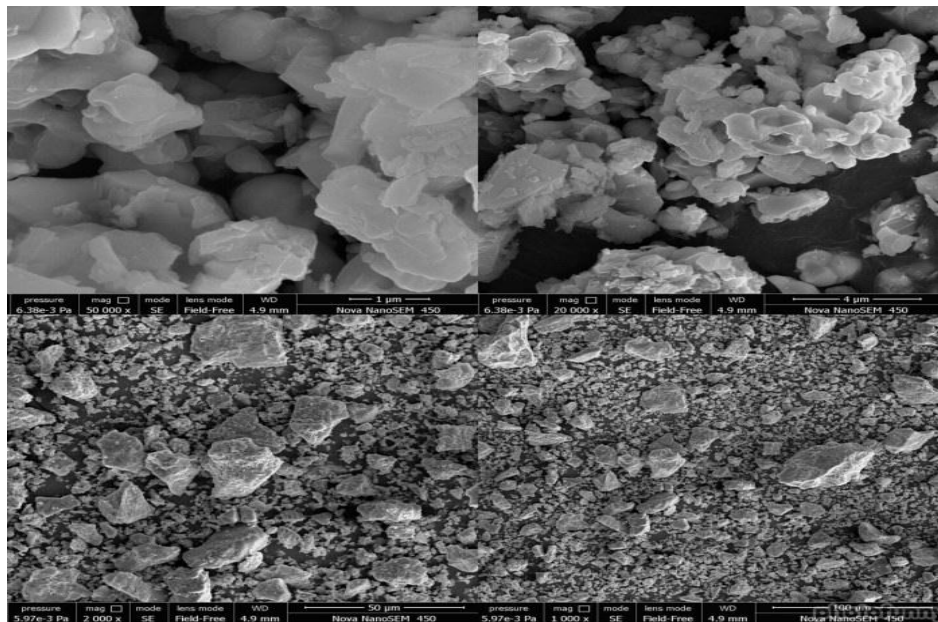


Figure 7: SEM micrograph of $Zn_{0.5}Mg_{0.5}Pr_{0.02}Fe_{1.98}O_4$

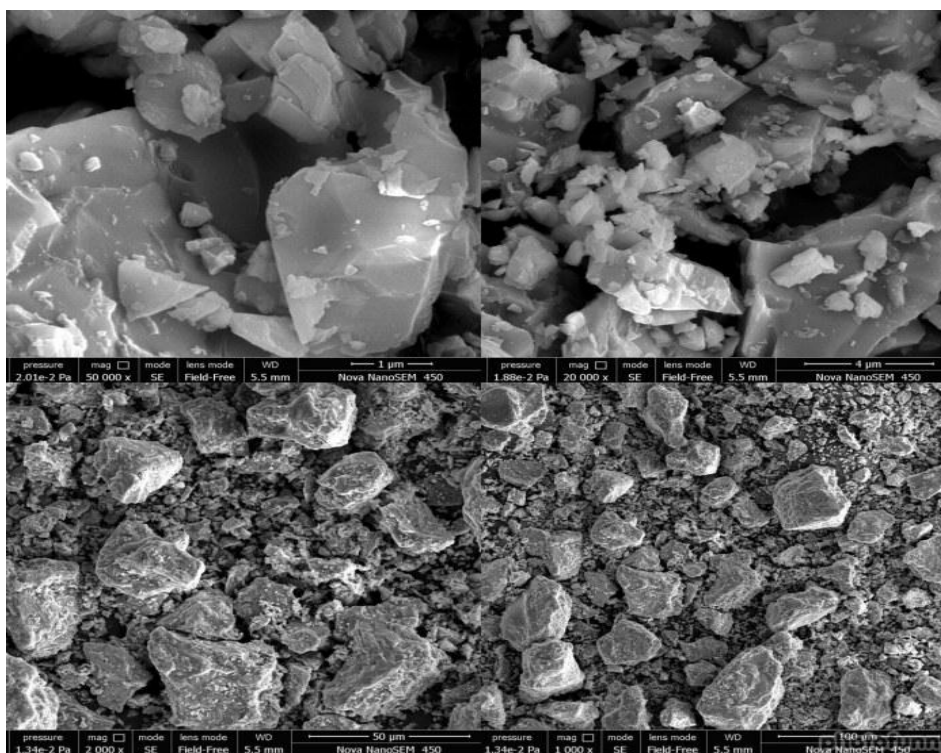


Figure 8: SEM micrograph of $Zn_{0.5}Mg_{0.5}Pr_{0.06}Fe_{1.94}O_4$

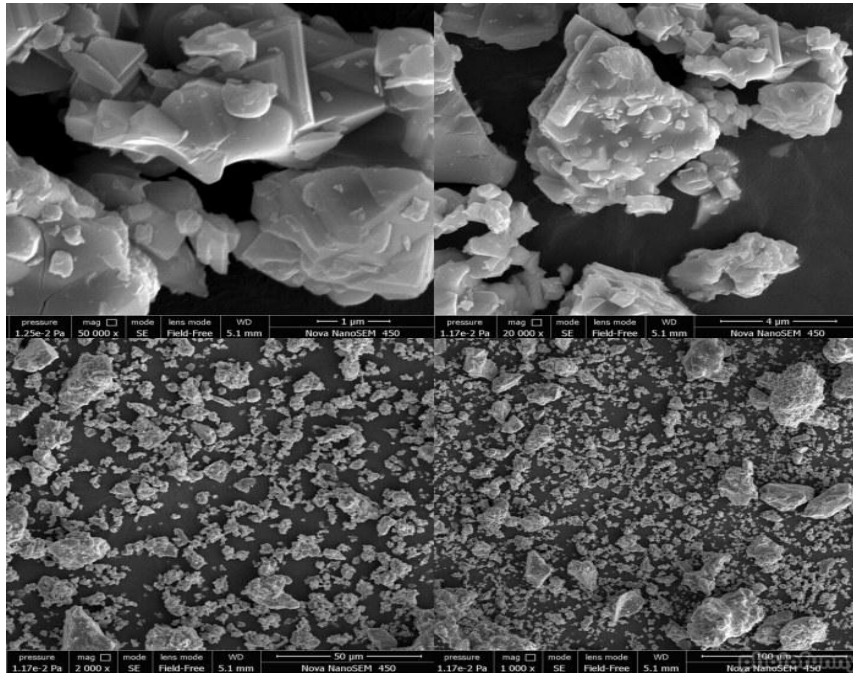


Figure 9: SEM micrograph of $Zn_{0.5}Mg_{0.5}Pr_{0.10}Fe_{1.90}O_4$

Figures 10-12 shows the EDS spectra of $Zn_{0.5}Mg_{0.5}Pr_xFe_{2-x}O_4$ (where $x=0.02, 0.06, 0.10$) ferrite sample. The occurrence of elements Zn, Mg, Fe, Pr and O has been

confirmed. Table 4 shows the values of atomic % matches approximately with the estimated values for the synthesized samples.

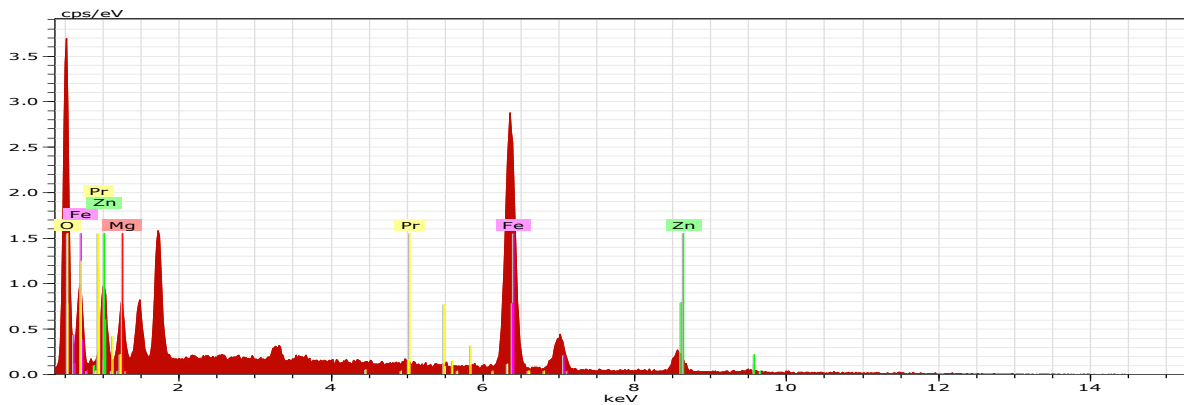


Figure 10: EDS spectra for $Zn_{0.5}Mg_{0.5}Pr_{0.02}Fe_{1.98}O_4$ ferrite.

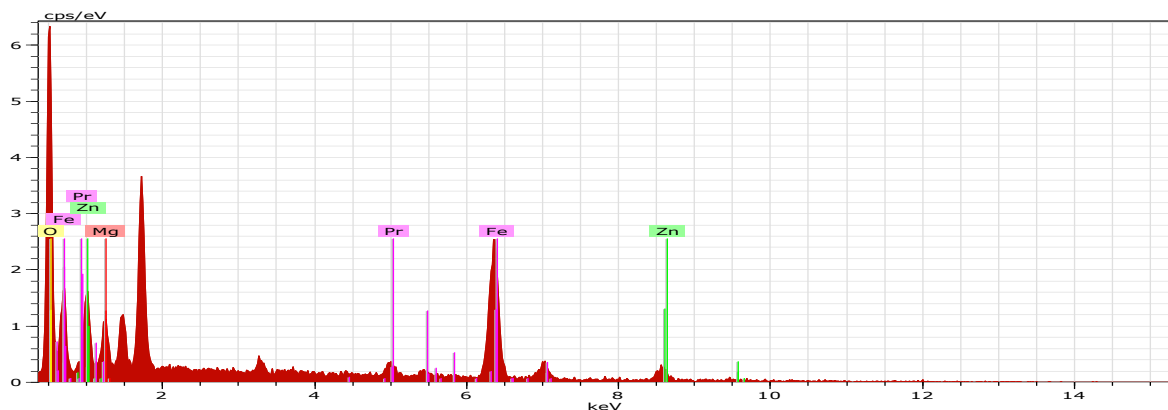


Figure 11: EDS spectra for $Zn_{0.5}Mg_{0.5}Pr_{0.06}Fe_{1.94}O_4$ ferrite.

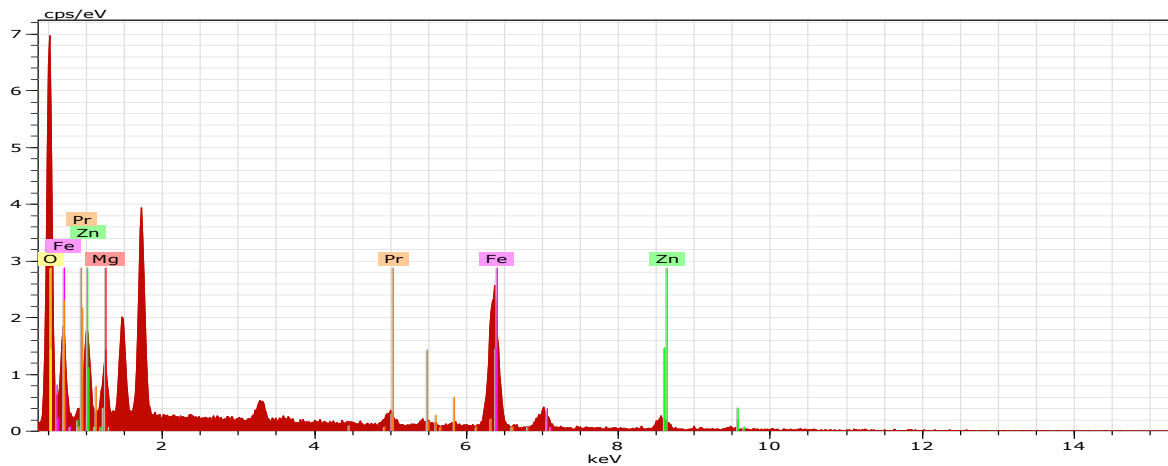


Figure 12: EDS spectra for $Zn_{0.5}Mg_{0.5}Pr_{0.10}Fe_{1.90}O_4$ ferrite.

Table 4: Values of atomic % for Pr^{3+} doped Zn-Mg ferrites

X	Atomic% Magnesium	Atomic % Zinc	Atomic % Iron	Atomic % Oxygen	Atomic % Praseodymium
0.02	4.99	13.93	58.97	19.86	2.24
0.06	5.18	15.30	44.25	28.21	7.06
0.10	5.36	14.85	42.10	31.05	6.65

The variation of dielectric constant of $Zn_{0.5}Mg_{0.5}Pr_xFe_{2-x}O_4$ (where $x=0.02, 0.06, 0.10$) with frequency (1 kHz-10MHz) at room temperature is shown in figure 13. From Figure we observed that as frequency increases, the dielectric constant decreases until it reaches a constant value at higher frequencies. The drop

in dielectric constant is particularly quick in the lower frequency area and becomes gradual as frequency increases [16]. The dielectric constant of ferrites is affected by the conduction process. The hopping of electrons between Fe^{2+} and Fe^{3+} is responsible for this conduction.

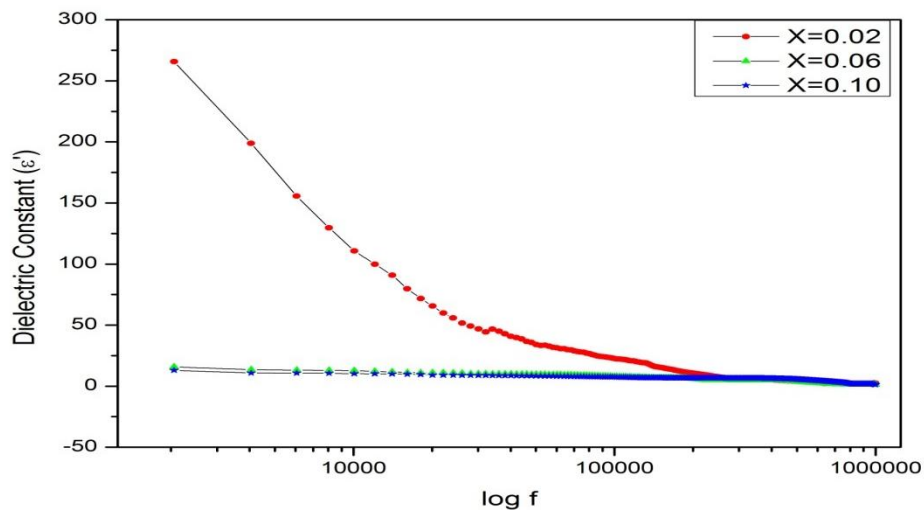


Figure 13: Dielectric constant versus $\log f$ curves for $Zn_{0.5}Mg_{0.5}Pr_xFe_{2-x}O_4$ at 300K.

The polarization exhibited at grain boundaries as a result of local charge displacement is mostly due to electron hopping. The Maxwell-Wagner model can explain such variations in dielectric constant with frequency in ferrites [17].

The dielectric structure of a ferrite material, according to this concept, is a mixture of two

layers. The first layer is made up of massive ferrite grains and serves as a conductive layer, whereas the second layer has grain boundaries that are poor conductors (offer high resistance). Hopping causes electrons to pile up at grain boundaries because to high resistance, resulting in polarization. At high frequencies, this hopping frequency does not follow the change

of the applied field. As a result, the dielectric constant at high frequencies remains constant.

The dielectric constant for free dipoles oscillating in an alternating field may be investigated as below-

Dipoles follow the applied field at extremely low frequencies where $\omega \leq 1/\tau$ (where τ is relaxation period) and $\epsilon' = \epsilon_s$ (ϵ_s dielectric constant at quasi static field). As the frequency, where $\omega < 1/\tau$, increases, dipoles do not follow the applied field and lag behind it, resulting in a reduction in dielectric constant. When the frequency reaches the characteristic frequency where $\omega = 1/\tau$, the dielectric constant decreases, indicating that the relaxation process has begun. Dipoles no longer follow the applied field at extremely high frequencies where $\omega \geq 1/\tau$, and $\epsilon' = \epsilon_\infty$ (ϵ_∞ is the high frequency value of ϵ'). Figure 11 depicts this trend by plotting a dielectric constant versus frequency plot. The figure shows that ϵ' is quite high at low frequencies and that as frequency increases, ϵ' decreases at first and later becomes constant. Normally, the dipolar electronic, ionic, and interfacial polarizations all contribute to a sample's dielectric constant. At low frequencies, dipolar and interfacial polarizations are effective. At higher frequencies, electronic polarization is effective for dielectric constant, and the contribution of dipolar polarisation is negligible. This dipolar relaxation process is the cause of high ϵ' at low frequencies. High values of ϵ' seen at extremely low frequencies can be attributed to charge accumulation at the interfaces inside the bulk of the sample, known

as interfacial polarisation or Maxwell Wagner polarisation, and at the interface between the sample and the electrode, known as space-charge polarisation.

Also from Figure 13 we saw that the value of the dielectric constant ϵ' decreases with the substituted ions of Pr^{3+} contents, which may be interpreted in the same way as the conduction process. The exchange of electrons between Fe^{2+} and Fe^{3+} ions causes local displacements between charges, which aids in the determination of charge polarisation in these ferrites. As a result, the quantity of Fe^{2+} ions on octahedral sites plays an important role in dielectric polarisation. Pr^{3+} ions occupy the octahedral position due to their greater ionic radius. Because of its steady valence, it impedes the conduction mechanism when Pr ions are substituted for iron ions (B-site). This implies that electron transfer cannot occur between Pr^{3+} and Fe^{2+} ions. As a result, the dielectric constant falls as dielectric polarisation decreases.

Figure 14 depicts the variation of dielectric loss of $\text{Zn}_{0.5}\text{Mg}_{0.5}\text{Pr}_x\text{Fe}_{2-x}\text{O}_4$ (where $x = 0.02, 0.06, 0.10$). Figure 14 clearly illustrates that the dispersion is similar to the dielectric constant. The loss tangent is considerable at low frequencies and becomes constant at high frequencies due to reduced polarisation at higher applied fields [18]. The observed fluctuation in loss tangent with frequency can be attributed to the ferrites, conduction process, which is similar to the Koop's phenomenological model [19].

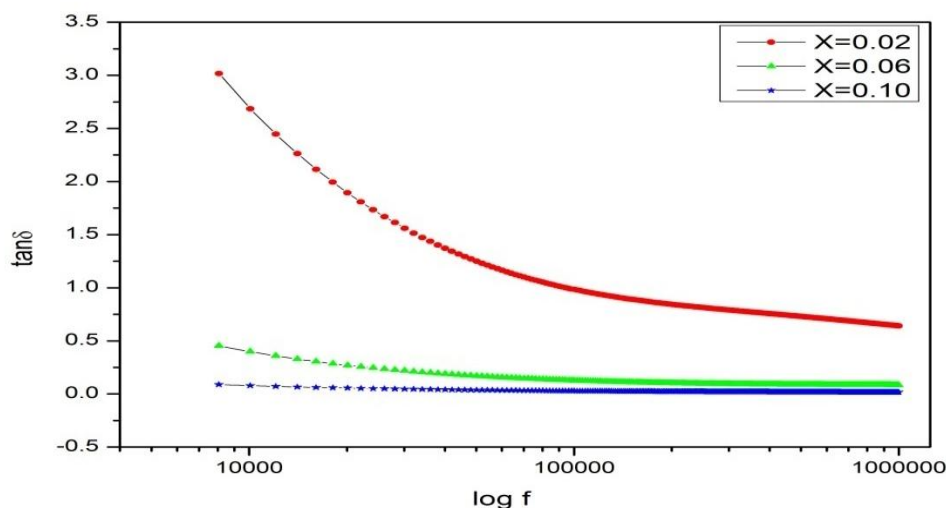


Figure 14: Dielectric constant versus log f curves for $\text{Zn}_{0.5}\text{Mg}_{0.5}\text{Pr}_x\text{Fe}_{2-x}\text{O}_4$ at 300K

According to the Koop's model, at lower frequencies, the impact of grain boundaries dominates, resulting in high resistivity and a high value of loss tangent. As a result, a significant quantity of energy is required for electron exchange between Fe^{3+} and Fe^{2+} ions, resulting in a significant amount of energy loss. At higher frequencies, however, a tiny amount of energy is required for electron exchange between Fe^{3+} and Fe^{2+} ions, resulting in a low resistivity and a minor amount of energy loss [20].

Figure 14 shows that the value of the loss tangent reduces as the concentration of Pr^{+3} increases, which is due to an increase in

resistivity as the concentration of Pr^{+3} increases.

The variation of impedance with frequency of $\text{Zn}_{0.5}\text{Mg}_{0.5}\text{Pr}_x\text{Fe}_{2-x}\text{O}_4$ (where $x=0.02, 0.06, 0.10$) ferrites are shown in figure 15.

Figure 15 shows that as frequency increases, the impedance decreases until it reaches a constant value at a higher frequency. The reduction in impedance is particularly quick in the lower frequency area and becomes gradual as frequency increases. Figures also show that the value of impedance increases with rising Pr^{+3} concentrations, which is owing to decreased dielectric polarization.

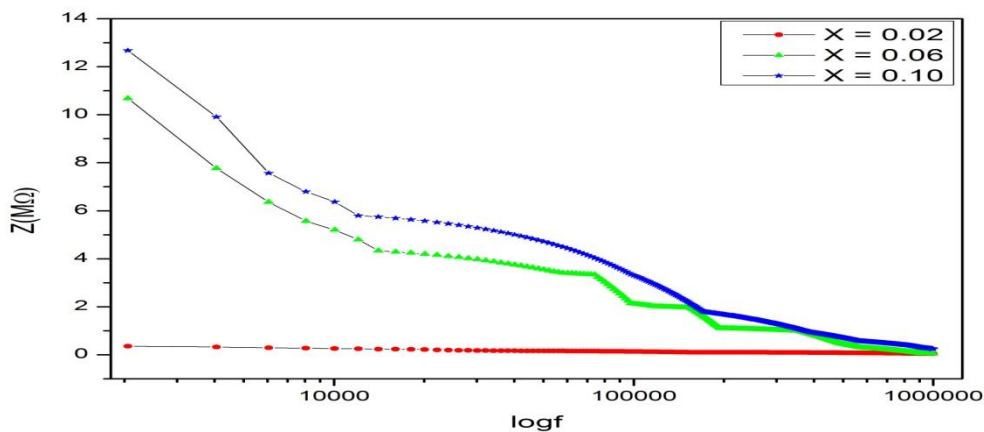


Figure 15: Impedance versus log f curves for $\text{Zn}_{0.5}\text{Mg}_{0.5}\text{Pr}_x\text{Fe}_{2-x}\text{O}_4$ at 300K.

Conclusion

$\text{Zn}_{0.5}\text{Mg}_{0.5}\text{Fe}_{2-x}\text{Pr}_x\text{O}_4$ (where $X = 0.02, 0.06, 0.10$) ferrite nanoparticles were synthesized successfully using high temperature solid state reaction technique. XRD patterns confirm the formation of spinel phase of ferrite samples along with secondary phases and with space group $\text{Fd}3\text{m}$. Lattice constant are increased with increase in Pr^{3+} ion concentration. FTIR spectra of the ferrite samples under investigation also reveal formation of single phase cubic spinel, showing two significant absorption bands ν_1 and ν_2 is ascribed to random variation of cations in the spinel structure. The method of preparation and nature of additives influence the cation distribution affecting the structural parameters. The grain size is calculated by SEM micrographs and observed that grain size is increases with increasing Pr concentrations.

The presence of Zn, Mg, Fe, Pr and O are confirmed by EDS. Dielectric constant, dielectric loss and impedance were measured as a function of frequency at room temperature. The dielectric constant and dielectric loss showing general nature of ferrites also observed that dielectric constant and dielectric loss were decreased with increasing the Pr concentrations while impedance increased with increasing Pr concentrations.

Acknowledgement

Authors are thankful to Department of Physics J. N. V. University Jodhpur for providing the XRD facility and Department of Physics M.L.S. University for providing dielectric measurements. One of the authors Shailendra Singh is thankful to UGC for providing the UGC-BSR doctoral fellowship.

References

1. Sheena Xavier, Smitha Thankachan, Binu P . Jacob and E. M. Mohammed,” Effect of sintering temperature on the structural and magnetic properties of cobalt ferrite nanoparticles”, *Nanosystems:Physics,Chemistry,Mathematics*, vol. 4(3), (2013), pp 430-437.
2. Veena Gopalan E, Al-Omari I A, Malini K A, Joy P A, Sakthi Kumar D, Yoshida Y and Anantharaman M R, “Impact of zinc substitution on the structural and magnetic properties of chemically derived nanosized manganese zinc mixed ferrites”, *Journal of Magnetism and Magnetic Materials*, vol. 321, (2009), pp 1092-1099.
3. Gorter E W, “Magnetization in Ferrites: Saturation Magnetization of Ferrites with Spinel Structure”, *Nature*, vol. 165, (1950), pp 798-800.
4. Gopalan V, Malini K A, Saravanan S, Sakthi Kumar D, Yoshida Y and Anantharaman M R, “Evidence for polaron conduction in nanostructured manganese ferrite”, *Journal of Physics D: Applied Physics*, vol. 41, (2008), pp 185005.
5. Srivastava M, Chaubey S and Ojha A K, “Investigation on Size Dependent Structural and Magnetic Behavior of Nickel Ferrite Nanoparticles Prepared by Sol-Gel and Hydrothermal Methods”, *Materials Chemistry and Physics*, vol. 174, (2009), pp 174-180.
6. H. Knoch, H. Dannheim, “Temperature dependence of the cation distribution in magnesium ferrite”, *Phys. Status Solidi A*, vol. 37(2), (1976), pp K135-K137.
7. Sun G-L, Li J-B, Sun J J and Yang X Z, “The influences of Zn^{2+} and some rare-earth ions on the magnetic properties of nickel-zinc ferrites”, *Journal of Magnetism and Magnetic Materials*, vol. 281(2-3), (2004), pp 173-177.
8. Rezlescu N, Rezlescu E, Pasnicu C and Craus M L, “Effects of the rare-earth ions on some properties of a nickel-zinc ferrite”, *Journal of Physics: Condensed Matter*, vol. 6.(1994), pp 5707.
9. Zhao L, Yang H, Zhao X, Yu L, Cui Y and Feng S, “Magnetic properties of $CoFe_2O_4$ ferrite doped with rare earth ion”, *Materials Letters*, vol. 60(1), (2006), pp 1-6.
10. Chakraverty S and Bandyopadhyay M, “Coercivity of magnetic nanoparticles: A stochastic model, *Journal of Physics: Condensed Matter*, vol. 19, (2007), pp 216201.
11. Shailndra Singh, Sahi Ram and S. K. Barbar, “Structural and Dielectric Studies of Dy Doped Zn-Mg Ferrite”, *AIP Conference Proceedings*, (2020), pp 080040-1–080040-4.
12. B. Rodriguez-Carvajal, “J. Recent developments of the program FULLPROF, in commission on powder diffraction. *IUCr. Newsletter*”, vol. 26, (2001), pp 12-19.
13. Shailndra singh, S. K. Barbar and Sahi Ram, “Synthesis and Characterization of Zn-Mg Ferrite”, *AIP Conf. Proc.*, 1953 (2018), pp 090023-1–090023-4.
14. R.D. Waldron, “Infrared spectra of ferrites”, *Physical Review*, vol. 99,(1955), pp 1727–1735
15. Anjali Verma, Ratnamala Chatterjee “Effect of zinc concentration on the structural, electrical and magnetic properties of Mn-Zn and Ni-Zn ferrites synthesized by the citrate precursor technique”, *Journal of Magnetism and Magnetic Materials*, vol.306, (2006), pp 313-320.
16. Jiagang Wu, John Wang, “Multiferroic behavior and impedance spectroscopy of bilayered $BiFeO_3 /CoFe_2O_4$ thin films”, *Journal of Applied Physics*, vol. 105, (2009), pp 124107.
17. M. Raghasudha, D. Ravinder, P. Veerasomaiah, “Influence of Cr^{3+} Ion on the Dielectric Properties of Nano Crystalline Mg-Ferrites Synthesized by Citrate-Gel Method”, *Material Science and Application*, vol. 4, (2013), pp 432-438.
18. N. Singh, A. Agarwal, S. Sanghi, S. Khasa, “Dielectric loss, conductivity relaxation process and magnetic properties of Mg substituted Ni-Cu ferrites”, *Journal of Magnetism and Magnetic Materials*, vol. 324,(2012), pp 2506.

19. M. L. Kahn, Z. J. Zhang, "Synthesis and magnetic properties of CoFe_2O_4 spinel ferrite nanoparticles doped with lanthanide ions", *Applied Physics Letter*, vol. 78, (2001), 3651-3653.
20. R. C. Kambale, P. A. Shaikh, C. H. Bhosale, K. Y. Rajpure, Y. D. Kolekar, "The effect of Mn substitution on the magnetic and dielectric properties of cobalt ferrite synthesized by an auto combustion route", *Smart Materials and Structures*, vol. 18, (2009), pp 115028.